Astronautics and Aeronautics, AIAA, Washington, DC, 1980, pp. 8–10.

[8]Vaught, C., Witt, M., and Netzer, D., "Investigation of Solid-Fuel, Dual-Mode Combustion Ramjets," *Journal of Propulsion and Power*, Vol. 8, No. 5, 1992, pp. 1004–1011.

[9]Zhongqin, Z., Zhenpeng, Z., Jinfu, T., and Wenlan, F., "Experimental Investigation of Combustion Efficiency of Air-Augmented Rockets," *Journal of Propulsion and Power*, Vol. 2, No. 4, 1986, pp. 305–310.

[10]Anil, K. N., and Damodaran, K. A., "Experimental Investigations on Flow Through a Petal Nozzle," *Journal of the Institute of Engineers, India*, Vol. 70, March, 1990, pp. 1–4.

[11]Anil, K. N., and Damodaran, K. A., "Mixing of Two Axisymmetric, Coaxial, High-Speed Streams with Heat Transfer," National Symposium on Experiments in Fluids, IIT Kanpur, India, Dec. 1992.

[12]Anil, K. N., "An Experimental Study on Mixing of Two Coaxial High Speed Streams," Ph.D. Dissertation, Aerospace Engineering, IIT Madras, India, Dec. 1992.

[13]Liepmann, H. W., and Roshko, A., *Fundamentals of Gas Dynamics*, Galcit Aeronautical Series, Wiley, New York, 1957.

Turbulent Combustion Regimes for Hypersonic Propulsion Employing Hydrogen-Air Diffusion Flames

G. Balakrishnan* and F. A. Williams†
University of California, San Diego, La Jolla, California 92093

Introduction

UNCERTAINTIES about turbulent combustion in hydrogen-air systems have an impact on our abilities to develop supersonic-combustion devices for applications such as the National Aerospace Plane. Most designs of supersonic-combustion engines involve turbulent hydrogen injection into supersonic airstreams in the combustor, thereby leading to nonpremixed combustion representative of turbulent diffusion flames. To begin combustor analyses it is helpful to have a firm identification of the regimes in which this turbulent combustion is likely to occur. The objective of the present communication is to report results of calculations performed to determine these combustion regimes.

Parameters Defining Regimes

A variety of nondimensional parameters are relevant to regimes of turbulent diffusion flames.[1,2] These include different Damköhler numbers, Reynolds numbers, convective Mach numbers (in compressible turbulence[1]), Zel'dovich numbers (measuring the strength of the temperature dependence of the chemistry), and the ratio of a rms mixture-fraction fluctuation to a reaction-zone width in mixture-fraction space (which is small in a connected-flamelet regime[3]). Of these, the most important for combustion is a large-eddy Damköhler number D_l, the ratio of a large-eddy turnover time $l/\sqrt{2k}$ (where l is the integral scale and k the kinetic energy of the turbulence), to a chemical time τ_c. Combustion occurs in a distributed-reaction regime for $D_l \ll 1$ and in a reaction-sheet regime for $D_l \gg 1$. The large-eddy Reynolds number $R_l = \sqrt{2k}l/\nu$, where ν is a kinematic viscosity, is also relevant in that turbulent structures appear in some sense to become truly fully developed for $R_l > 10^4$. Other Damköhler and Reynolds numbers that may be considered are D_k, the ratio of the Kolmogorov time to τ_c, and R_t, the Reynolds number based on the Taylor scale.

Figure 1 is a plane having R_l and D_l as coordinates, for the purpose of exhibiting turbulent combustion regimes.[4] The influence of parameters such as Mach number and Zel'dovich numbers do not fit well in this plane; in principle they require extension to additional dimensions. However, since the combustion regimes are so strongly influenced by the chemical and flow times, the Damköhler and Reynolds number may be deemed the two most significant parameters, and therefore, to leading order this plane may serve as groundwork for regimes. Plotted on this plane are lines of constant values of other parameters, fully discussed earlier,[4] that are relevant mainly for premixed turbulent combustion, as are the multiple, single, and weak-turbulence subregimes. The results reported here concern the location in this plane of projected supersonic-combustion processes for hypersonic air-breathing propulsion employing hydrogen as fuel.

Specification of Flight Parameters

Flight Mach numbers M_f from 1 to 25 are considered at altitudes from 11 to 80 km, with the U.S. standard atmosphere (NOAA, 1976). An average diffuser efficiency of 95% (recommended by engine manufacturers) is employed, with combustor air Mach numbers of $M_f/2$ for $M_f \leq 4$ and $M_f/2 - 1$ for $M_f > 4$, fuel-stream Mach numbers from 1 to 4, temperatures from 300 to 1200 K, and a characteristic combustor dimension of 0.3 m. Resulting combustor static pressures range from 0.3 to 5.0 atm.

The chamber static temperature and pressure are first calculated for any given altitude and M_f from standard quasi-one-dimensional gasdynamic formulas, and ν is then obtained from NASA polynomial fits, using the average of the static temperature and the diffusion-flame extinction temperature[5] as a first estimate, since temperatures in the regions of flow where ν is relevant are distributed between these limits. The turbulence intensity is approximated as 50%, and the integral scale as the chamber dimension for the purpose of estimating

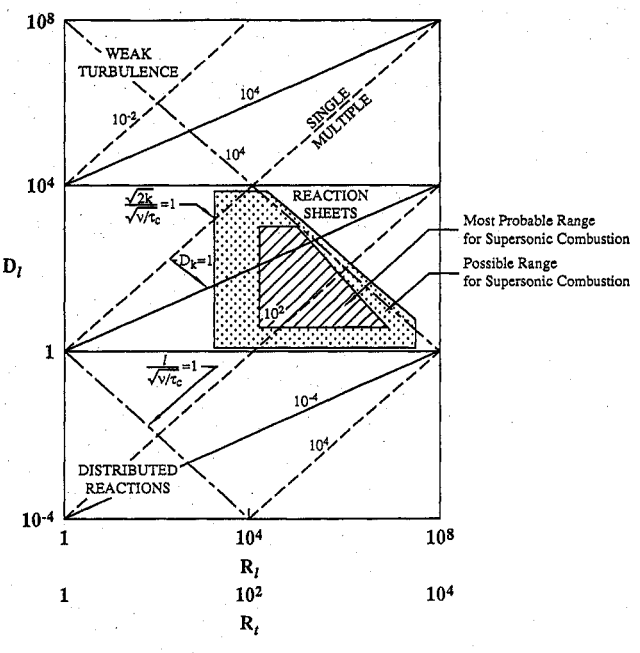

Fig. 1 Diagram of the regimes of turbulent combustion.

Received July 26, 1993; revision received Dec. 6, 1993; accepted for publication Dec. 13, 1993.

*Assistant Project Scientist, Center for Energy and Combustion Research.

†Professor of Engineering Physics, Center for Energy and Combustion Research. Fellow AIAA.

Table 1 Specific reaction-rate constants for the hydrogen-oxygen system adopted in the present study

No.	Reactions	A^a	n^a	E^a	Source
1	$H + O_2 \rightleftharpoons OH + O$	3.52×10^{16}	−0.7	17070	Mansten et al.[13]
2	$H_2 + O \rightleftharpoons OH + H$	5.06×10^{4}	2.67	6290	Yetter et al.[15]
3	$OH + OH \rightleftharpoons H_2O + O$	$k = 5.46 \times 10^{11} \exp(0.00149T)$			Yetter et al.[15]
4	$H_2 + OH \rightleftharpoons H_2O + H$	1.17×10^{9}	1.3	3626	Baulch et al.[14]
5[b]	$H + O_2 + M \rightleftharpoons HO_2 + M$	6.76×10^{19}	−1.42	0	Yetter et al.[15]
6	$H + HO_2 \rightleftharpoons OH + OH$	1.70×10^{14}	0.0	874	Baulch et al.[14]
7	$H + HO_2 \rightleftharpoons H_2 + O_2$	4.28×10^{13}	0.0	1411	Baulch et al.[14]
8	$OH + HO_2 \rightleftharpoons H_2O + O_2$	2.89×10^{13}	0.0	−497	Baulch et al.[14]
9[c]	$H + H + M \rightleftharpoons H_2 + M$	1.80×10^{18}	−1.0	0	Smooke[16]
10[b]	$H + OH + M \rightleftharpoons H_2O + M$	2.20×10^{22}	−2.0	0	Baulch et al.[14]
11	$HO_2 + HO_2 \rightleftharpoons H_2O_2 + O_2$	3.02×10^{12}	0.0	1390	Yetter et al.[15]
12[d]	$H_2O_2 + M \rightleftharpoons OH + OH + M$	1.20×10^{17}	0.0	45500	Yetter et al.[15]
13	$H_2O_2 + OH \rightleftharpoons H_2O + HO_2$	7.08×10^{12}	0.0	1430	Yetter et al.[15]
14	$O + HO_2 \rightleftharpoons OH + O_2$	2.00×10^{13}	0.0	0	Baulch et al.[14]
15	$H + HO_2 \rightleftharpoons O + H_2O$	3.10×10^{13}	0.0	1720	Baulch et al.[14]
16[b]	$H + O + M \rightleftharpoons OH + M$	6.20×10^{16}	−0.6	0	Yetter et al.[15]
17[b]	$O + O + M \rightleftharpoons O_2 + M$	6.17×10^{15}	−0.5	0	Yetter et al.[15]
18	$H_2O_2 + H \rightleftharpoons H_2O + OH$	1.00×10^{13}	0.0	3590	Smooke[16]
19	$H_2O_2 + H \rightleftharpoons HO_2 + H_2$	4.79×10^{13}	0.0	7950	Smooke[16]
20	$O + OH + M \rightleftharpoons HO_2 + M$	1.00×10^{16}	0.0	0	Smooke[16]
21	$H_2 + O_2 \rightleftharpoons OH + OH$	1.70×10^{13}	0.0	47780	Smooke[16]

[a]Units: mol/cm^3, s^{-1}, K, cal/mol; rates for reverse steps obtained from JANAF thermochemical equilibrium data.
[b]Chaperon efficiencies: H_2: 2.5, H_2O: 12.0, O_2: 1.0 and N_2: 1.0.
[c]Chaperon efficiencies: H_2: 1, H_2O: 6.5, O_2: 0.4 and N_2: 0.4.
[d]Chaperon efficiencies: H_2: 2.5, H_2O: 15.0, O_2: 1.0 and N_2: 1.0

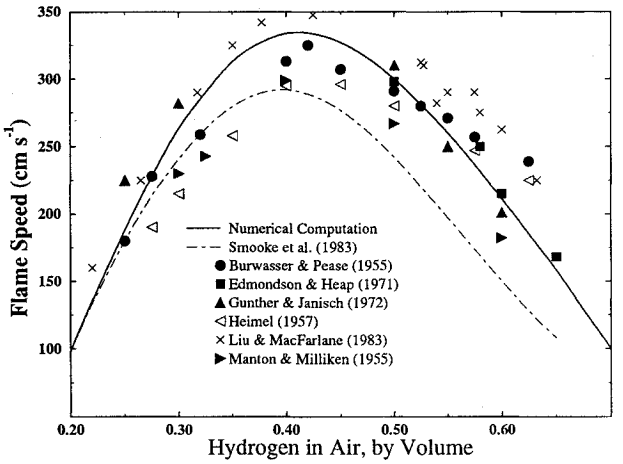

Fig. 2 Effect of hydrogen concentration on burning velocity for premixed hydrogen-air flames at 1 atm and initially at 300 K.

R_l and $l/\sqrt{2k}$. Determination of τ_c as described below then enables D_l to be calculated and the regimes to be drawn on Fig. 1.

Chemical Time

The selection of τ_c depends on both the character of the combustion process and the turbulent combustion regime. In the distributed-reaction regime, the sum of an ignition time and a heat-release time is appropriate, whereas in reaction-sheet regimes, the ratio of a thermal diffusivity to the square of a laminar flame speed applies under premixed conditions and the reciprocal of a strain rate for laminar diffusion-flame extinction under nonpremixed conditions. These various overall chemical times can be calculated from the rates of the elementary reaction steps. Currently updated specific reaction-rate constants in the form $k = AT^n \exp(-E/RT)$ are listed in Table 1; rates of reverse steps are evaluated from equilibrium constants. These rates are now known accurately enough that their errors are unlikely to introduce significant uncertainties into estimated regimes. The computed laminar flame speed as a function of the hydrogen content in air at 1 atm and initially at 300 K, shown in Fig. 2, is an illustration of the good agreement with experiment[6–12] that supports the validity of this rate data.

The rate constants of Table 1 have been selected to apply for temperatures between 300–3000 K and pressures between 0.25–40 atm, which encompasses the relevant conditions for the application, as given above. "Falloff" effects, i.e., effective variations of reaction orders with pressure, are not included here because they are unlikely to be significant for these elementary steps over the pressure range considered. Of particular interest in Table 1 is the rate of the most important chain-branching reaction $H + O_2 \rightarrow OH + O$ which is based on the recent Stanford shock-tube experiments.[13] The new rate provides a slightly larger radical pool, and unlike the rate recommended by Baulch et al.[14] in their recent review, exhibits the correct direction of the temperature dependence for the reverse reaction $OH + O \rightarrow H + O_2$, in the temperature range 500–3000 K. The non-Arrhenius fit recommended by Yetter and his coworkers[15] for the shuffle reaction $OH + OH \rightarrow H_2O + O$ is used since it seems to provide better agreement with the experimental data over this temperature range.

The mechanism of Table 1 involves eight reactive species, namely, H_2, O_2, H, O, OH, HO_2, H_2O, and H_2O_2. Tests have shown that steps 14–21 of the mechanism are negligible to a great extent,[5] so that a 13-step mechanism is sufficient. Nevertheless, the computations whose results are used here employed the 21-step mechanism for completeness. The largest difference from prediction with the 13-step mechanism for the structures of counterflow diffusion flames amounts to about a 20% lower peak H_2O_2 concentrations with the fuller mechanism; differences are observable only for HO_2 and H_2O_2 profiles. The H_2O_2 pathways are relevant in determining critical ignition parameters at low temperatures and high pressures, bordering on the range of interest in the application. In general, the recommended rate constants in Table 1 were obtained through comparative evaluations of the differing results of the four sources identified there and through estimates of errors and uncertainties in these sources.

If combustion occurs in the reaction-sheet regime in the present application, then the strain rate determines the flow time, so that $\tau = K/a_e$ is appropriate, where a_e is the component, normal to the reaction sheet, of the oxidizer-side strain rate for the extinction of laminar axisymmetric counterflow diffusion flamelets, and K is a constant. Based on the

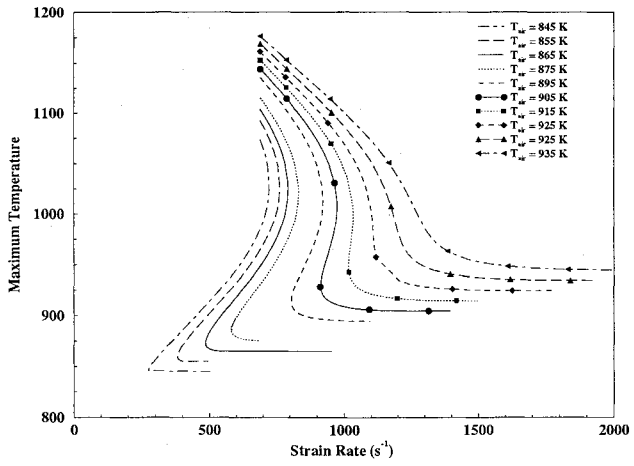

Fig. 3 Dependence of the maximum temperature on strain rate for a diluted hydrogen-air flame with a hydrogen mole fraction of 0.16 in the hydrogen-nitrogen fuel feed, a temperature of the fuel stream of 298 K, various airstream temperatures, and a pressure of 0.25 atm.

work of Seshadri and Peters,[17] a correspondence for hydrogen flames was developed by Peters,[18] giving $K \approx 0.2$. An alternative simple estimate is $K = 1$. In the present work, the intermediate value of $K = \frac{1}{2}$ is employed. The differences of these various estimates contribute to the uncertainty of the estimated regimes as indicated below.

Extensive numerical computations of counterflow diffusion-flame structure and extinction were completed with the preceding reaction scheme, over the range of pressures and temperatures identified above.[5] Representative results of computations are shown in Fig. 3. The results were employed for obtaining τ_c to evaluate D_l.

Results and Discussion

The results of the calculations are shown in Fig. 1. In this figure, the "most probable region" is the range of estimates obtained as described above. It is seen from the discussion in the previous section that the largest uncertainties in evaluating the Damköhler number D_l arise from the uncertainties in estimating the chemical time τ_c. However, the uncertainties in ν and k predominantly affect the possible range for the turbulent Reynolds number R_l. The kinematic viscosity ν strongly depends on the temperature and the composition of the mixture, and for most of the operating range increases rapidly from the cooler fuel stream to the hot airstream. In estimating the "most probable range," influences of heat release on the turbulent kinetic energy k are neglected, although previous research[19] suggests a possible decrease in the turbulent fluctuations associated with the expansion of gases caused by heat release. This effect, which introduces further uncertainties in R_l, is mitigated, however, at high Mach numbers through compressible heating.[1] The "possible range" shown in Fig. 1 is the broader range obtained with these uncertainties in τ_c, ν, l, k, and diffuser efficiency (taken as 90–98%) included. It is seen that these estimates give approximately $1 < D_l < 10^4$ and $10^4 < R_l < 10^8$. Fully developed turbulence and reaction-sheet regimes are therefore predicted by these calculations.

It is worth noting that there are critical strain rates for laminar diffusion-flame ignition to occur, and these strain rates are less than those for extinction, as illustrated in Fig. 3. If these ignition strain rates were used, then τ_c would be larger and D_l would be smaller. Moreover, autoignition times are infinite at these critical ignition strain rates, and even lower strain rates are needed to produce ignition times comparable with τ_c obtained from the extinction strain rate. Since turbulent diffusion flames, once they exist in the chamber, provide sufficient concentrations of radicals to make autoignition computations irrelevant, there is uncertainty concerning how important the ignition estimates may be for determining regimes.

A sufficiently wide range of transient ignition histories has not yet been calculated to test whether an assumption that combustion occurs in the distributed-reaction regime can be self-consistent for these applications. When ignition begins to become controlling, the rates tend to become highly sensitive to local conditions such as local temperature, and combustion efficiencies can rapidly become very low. Such conditions are detrimental and must be avoided. Certain ranges of parameters might therefore have to be excluded in practice. Further computations are needed to identify these ranges. When the combustor performs well, the diffusion-flame calculations reported here should apply, and the corresponding estimates of the regimes may then be accepted.

An implication of these results is that, in motor designs, computational methods for turbulent combustion based on reaction-sheet rather than distributed-reaction concepts are most realistic for well-performing supersonic-combustion engines employing hydrogen fuel in air.

Acknowledgment

This work was supported by the Air Force office of Scientific Research under Grant F49620-92-J-0184.

References

[1]Libby, P. A., and Williams, F. A. (eds.), *Turbulent Reacting Flows*, Academic Press, London, 1994.

[2]Liñán, A., and Williams, F. A., *Fundamental Aspects of Combustion*, Oxford Univ. Press, New York, 1993.

[3]Peters, N., "Laminar Flamelet Concepts in Turbulent Combustion," *Twenty-First Symposium (International) on Combustion*, The Combustion Inst., Pittsburgh, PA, 1987, pp. 1231–1250.

[4]Williams, F. A., "Turbulent Combustion," *The Mathematics of Combustion*, edited by J. Buckmaster, Society for Industrial and Applied Mathematics, Philadelphia, PA, 1985, pp. 97–131.

[5]Balakrishnan, G., "Studies of Hydrogen-Air Diffusion Flames and of Compressibility Effects, Related to High Speed Propulsion," Ph.D. Dissertation, Univ. of California, San Diego, La Jolla, CA, Sept. 1992.

[6]Smooke, M. D., "Solution of Burner-Stabilized Premixed Laminar Flames by Boundary-Value Methods," *Journal of Computational Physics*, Vol. 48, Oct. 1982, pp. 72–105.

[7]Burwasser, H., and Pease, R. N., "The Burning Velocity of Hydrogen-Air Flames," *Journal of the American Chemical Society*, Vol. 77, No. 5, 1955, pp. 5806–5808.

[8]Edmondson, H., and Heap, M. P., "The Burning Velocity of Hydrogen-Air Flames," *Combustion and Flame*, Vol. 16, No. 1, 1971, pp. 161–165.

[9]Günther, R., and Janisch, G., "Measurements of Burning Velocity in a Flat Flame Front," *Combustion and Flame*, Vol. 19, No. 1, 1972, pp. 49–53.

[10]Heimel, S., "Effect of Initial Mixture Temperature on Burning Velocity of Hydrogen-Air Mixtures with Preheating and Simulated Preburning," NACA TN-4156, March 1957.

[11]Liu, D. D. S., and MacFarlane, R., "Laminar Burning Velocities of Hydrogen-Air and Hydrogen-Air-Steam Flames," *Combustion and Flame*, Vol. 49, No. 1, 1983, pp. 59–71.

[12]Manton, J., and Milliken, B., "Study of Pressure Dependence of Burning Velocity by the Spherical Vessel Method," *Proceedings of the Gas Dynamic Symposium (Aerothermochemistry)*, Northwestern Univ., Evanston, IL, 1955, pp. 151–158.

[13]Masten, D. A., Hanson, R. K., and Bowman, C. T., "Shock-Tube Study of the Reaction $H + O_2 \rightarrow OH + O$ Using Laser Absorption," *Journal of Physical Chemistry*, Vol. 94, No. 18, 1990, pp. 7119–7128.

[14]Baulch, D. L., et al., "Evaluated Kinetic Data for Combustion Modelling," *Journal of Physical and Chemical Reference Data*, Vol. 21, No. 3, 1992, pp. 411–736.

[15]Yetter, R. A., Dryer, F. L., and Rabitz, H., "A Comprehensive Reaction Mechanism for Carbon Monoxide/Hydrogen/Oxygen Kinetics," *Combustion Science and Technology*, Vol. 79, Nos. 1–3, 1991, pp. 97–128.

[16]Smooke, M. D. (ed.), *Reduced Kinetic Mechanisms and Asymptotic Approximations for Methane-Air Flames*, Springer-Verlag, New York, 1991.

[17]Seshadri, K., and Peters, N., "Asymptotic Structure and Extinction of Methane-Air Diffusion Flames," *Combustion and Flame*, Vol. 73, No. 1, 1988, pp. 23–44.

[18]Peters, N., "Length Scales in Laminar and Turbulent Flames," *Numerical Approaches to Combustion Modeling*, edited by E. S. Oran and J. P. Boris, Progress in Aeronautics and Astronautics, AIAA, Washington, DC, 1991.

[19]Libby, P. A., and Williams, F. A. (eds.), *Turbulent Reacting Flows*, Springer-Verlag, New York, 1980.

Technical Comments

Comment on "Simple Modeling of Particle Trajectories in Solid Rocket Motors"

John W. Murdock*
The Aerospace Corporation, Los Angeles, California 90009

THE subject paper[1] presents a method for computing slag capture in a solid rocket motor that decouples the gas-particle interaction. First, a potential flow model is used to compute the gas flowfield; second, a Lagrangian particle tracking scheme computes the trajectories of the condensed phase. Since the slag capture is determined by the particle paths, which in turn depend on the gas-dynamic drag, an accurate flowfield is a necessary component of the method. This Comment questions the assumption that the gas flow is potential on both theoretical and experimental grounds, and suggests that an inviscid, vortical flow is more appropriate. In addition, an analytical comparison of the potential flow solution with the vortical solution advocated herein for a geometry typical of a solid rocket motor shows that the gas velocities predicted by the two methods may differ by more than an order of magnitude and by nearly 90 deg at selected locations.

Reference 1 is one in a series of three papers by the same group of authors.[2,3] All use the same assumptions to address slag capture issues. Interestingly, the authors of Refs. 1–3 are aware of and cite Culick's[4] 1966 paper, which showed that in order to properly satisfy the flow boundary conditions at a solid-propellant burning surface, a vortical solution was required. Culick compares the analytical solutions for vortical and potential flows in a constant bore radius motor and states that "a better approximation, more consistent with the burning process, should satisfy the condition that the velocity is normal to the surface."

Most of the arguments in favor of using the potential flow model for the gas are contained in the first[1] of the three papers. One of these arguments,[1] that cites Bachelor[5] for support, states that the specification of the vorticity in the solid-motor inviscid flow is arbitrary. A careful reading of Bachelor indicates that he is referring to the two-dimensional equation with vorticity, but without imposition of the boundary conditions, when he states the "vorticity distribution is arbitrary, so far as inviscid-fluid theory is concerned."[5] Furthermore, he notes the constancy of the vorticity along inviscid streamlines, thus limiting any arbitrariness. Hence, the two-dimensional differential equation, plus the two components of the velocity vector specified at the propellant surface, constitute a well-posed, boundary-value problem by implicitly defining the vorticity on each streamline. One way to show that this problem is well posed is to consider the incompressible, inviscid, two-dimensional, primitive-variable formulation of the fluid equations and use the methods of Courant and Hilbert[6] to find the characteristics. A single real characteristic is found, which coincides with the streamlines, in addition to the two imaginary characteristics associated with the simpler, potential flow. Thus, an additional boundary condition above and beyond the usual potential flow condition is required at boundary locations where streamlines enter the solution region. In the present case, this condition is, as suggested by Culick,[4] that the tangential velocity at the propellant surface is zero.

A subsequent argument in favor of the use of potential flow invokes Goldstein's[7] work on boundary-layer theory. It is stated that "Conventionally for inviscid flow, a vortex sheet is introduced at the boundary to enforce zero slip."[1] One must be careful in applying boundary-layer theory to the flow inside rocket motors. In the case of a boundary layer on a solid, impermeable surface, a vortex sheet indeed can be introduced to enforce zero slip at the wall. With the viscosity neglected, this vorticity does not enter the flowfield, since the convective velocity is tangent to the vortex sheet and the normal diffusion has been neglected. This inviscid solution is irrotational only outside the vortex sheet and satisfies the wall boundary conditions on both components of the velocity. Also, it is a first approximation to the complete solution if the viscosity is small and the boundary layer thin. When the viscosity is small but non-negligible, the vortex sheet diffuses and convects to form the usual boundary layer. However, in the case of interest here, the flow boundary is not a solid surface but is a propellant burning surface. Hence, a solution with a vortex sheet at the boundary is not a valid first approximation to the flow, because the flow is not parallel to the vortex sheet. The vorticity is immediately convected into the flowfield. Therefore, a potential flow with a vortex sheet at an inflow boundary (a propellant burn surface) is not a valid approximation for even the inviscid flow.

Theoretical considerations aside, there is experimental validation of the Culick[4] vortical formulation by Dunlap and his coworkers[8,9] that has been overlooked by the authors of the subject papers. In the earlier paper,[8] it is pointed out that the vortical flow solution advocated herein is an inviscid solution of the incompressible flow equations that satisfies the viscous boundary conditions. Therefore, it is concluded that the solution should agree with real flows if the Reynolds number is large. Laminar flow data are presented for a simulated constant radius motor in the Reynolds number range 3×10^3 to 24×10^3 that are in excellent agreement with Culick's[4] model. The second[9] of these papers provides further experimental validation of the theoretical model; the laminar flow results of the previous paper[8] in which the viscous effects are negligible are confirmed. For turbulent flow, it is found that the pressure force still is larger than the shear force, but only by a factor varying between 2–10. The result is that the measured turbulent velocity profiles agree with the theoretical inviscid solutions in the core flow region, but there is some deviation near the wall where the shear is highest. Figure 21 of Ref. 9 shows that the measured centerline flow velocity drops about 5% below the linear, vortical, inviscid prediction due to turbulence; the predicted, potential-flow, centerline

Received July 3, 1993; revision received Sept. 17, 1993; accepted for publication Sept. 27, 1993.

*Manager, Fluid Mechanics Technology Section. Associate Fellow AIAA.